Chemical Data Collections 33 (2021) 100683

Contents lists available at ScienceDirect

Chemical Data Collections

journal homepage: www.elsevier.com/locate/cdc

Data Article

Data on electrochemical deterioration of mild steel in rice husk agro-waste developed nano-coolant

Sunday A. Afolalu[a], Olufunmilayo O. Joseph[a,*], Olabisi O. Yusuf[b], Moses E. Emetere[c]

[a] Department of Mechanical Engineering, Covenant University, P.M.B. 1023, Ota, Nigeria
[b] Department of Microbiology, Obafemi Awolowo University, Ile-Ife, Nigeria
[c] Department of Physics, Covenant University, Ota, Nigeria

ARTICLE INFO

Article history:
Received 1 September 2020
Revised 20 January 2021
Accepted 16 March 2021
Available online 17 March 2021

Keywords:
Nano-coolant
Agro-waste
Nano-fluid
Nanoparticles
Cutting fluid

ABSTRACT

Investigation of the electrochemical deterioration of mild steel in rice husk agro-waste developed nano-coolant is presented in this study. Corrosion rates of mild steel versus nano-coolant concentration are presented. Linear polarization test data was also covered. Mild steel coupons were immersed in different concentrations (ten concentrations and the control as a reference) of the developed nano-fluid for a period of 24, 48, 72, 96, 120, 144 and 168 h. Corrosion rate was calculated based on ASTM Standard G1–03 standard practice for preparing, cleaning and evaluation of corrosion test specimens. Open circuit potential measurements (OCP) were also carried out. The potential of the steel samples in the nano-fluid with respect to time was investigated. This dataset could be used in evaluating the performance of mild steel in rice husk based nano-coolant.

Specifications Table

Subject area	Materials Science and Engineering
Compounds	Rice husk ash, water
Data category	Physicochemical
Data acquisition format	JSM-7600F Schottky Field Emission Scanning Electron Microscope coupled with energy dispersion spectrometer, Digi-Ivy potentiostat.
Data type	Raw, analyzed
Procedure	Open circuit potential tests and linear sweep voltametry via potentiostatic analysis, weight loss measurements, corrosion rate determination
Data accessibility	Data are available within this article

1. Rationale

During machining operations, a metalworking fluid is introduced to create a film on the surfaces in contact providing a means of lubrication and acts as a medium for cooling in order to dispel the generated heat. While doing so, they flush

* Corresponding author.
E-mail address: funmi.joseph@covenantuniversity.edu.ng (O.O. Joseph).

https://doi.org/10.1016/j.cdc.2021.100683

Table 1
Nano-fluid concentration for each test condition.

SAMPLE	NANO FLUID (g/Litre)
RH-A	0.10
RH-B	0.20
RH-C	0.25
RH-D	0.50
RH-E	0.75
RH-F	1.00
RH-G	1.25
RH-H	1.50
RH-I	2.00
RH-J	2.50
RH-K	CONTROL

away the chips formed during the machining operation [1,2]. Shokoohi et al. [3] described cutting fluids as a medium used to reduce the metal to metal contact between the tool and work piece thereby preventing internal friction during machining operations. Cutting fluids are introduced in order to eliminate heat from the chips, tool and work piece thereby cooling it in the process preventing temperature build-up. According to [4,5] cutting fluids should be capable of preventing the tool from being heated to a temperature where its hardness will be reduced. They should also serve as corrosion inhibitors thereby protecting the piece from rusting and improving the surface finish of the piece. In order to enhance the thermo-physical properties of fluids, millimeter or micrometer sized solid particles were added to base fluids. However, due to the large size of the particles, they ended up clogging surfaces, causing abrasion, rust and a series of other problems hence, they were not suited for practical use. Over time, through research and advancement in technology, the development of nano-fluids has made that possible [6–11]. Unlike the regular solid-liquid suspension, nano-fluids possesses higher specific surface area and higher dispersion stability. Nano-fluids also demonstrate the benefit of refining surface roughness thereby averting burning of the workpiece [12]. Furthermore, every year, a large amount of agricultural by-products such as fruit peels, grain husks, nut shells, etc. are discarded in landfills. About 90% of the time, these products are burnt then left to decay or used for mulching leaving behind toxic fumes. However, the ash left behind from the remains of some of these products are rich in carbon, silica and other components which have many applications in a lot of technological fields [11,13–16]. Hence, in support of the quest to create a clean and sustainable environment, agricultural wastes are being utilized in the development of nano-fluids [17,18]. This dataset seeks to project the performance of rice husk as an agro-industrial waste product in the development of a nano-cutting fluid which is environmentally sustainable, clean, non-toxic and contributes to green machining.

The data for the mass loss corrosion rates can be used to predict the corrosion rates of immersed samples. Data on mass loss corrosion rates can increase knowledge base on how silica based nano-cutting fluids affect materials during machining operations. The data on open circuit potential (OCP) can be used to determine the potential at which the cathodic and anodic reaction rates are in equilibrium in the developed nano-coolant. The data acquired for OCP can be used to predict the thermodynamic tendency of the mild steel material to participate in electrochemical corrosion reactions within the nano-cutting fluid. The data for linear polarization gives a hint regarding the corrosion resistance of mild steel in the nano-cutting fluid [19–23].

2. Procedure

Firstly, the rice husk was washed using water to get rid of impurities, sand, etc. then it was sun dried for 10 h after which it was burnt into ashes using a muffle furnace at 500 °C for 12 h. A black ash was obtained which was left to cool for about 12 h. Afterwards, the rice husk ash was ground into a coarse powder then milled using a planetary ball mill. The resulting ash obtained was of a fine consistency and was used as the base for the silica nanoparticle synthesis. The Silica nanoparticles were synthesized from the agro waste source (Rice Husk Ash) using the chemical synthesis method. Sodium hydroxide (NaOH) was used as the precursor salt for this method. 10 g of the Rice Husk Ash (RHA) was mixed with a solution of 40 g of Sodium hydroxide (NaOH) pellets and 1000 ml of distilled water to create an aqueous solution. This solution was then stirred using a Stuart US 152 heat-stir magnetic stirrer/ hot plate for 4 h at 100 °C. After stirring, the solution obtained was left to cool to room temperature then was titrated using 485 ml of 10% H_2SO_4 until it was neutralized to a pH of 7.

The solution obtained at the end of the reaction process was poured into 10 ml centrifuge tubes where it was spun in a JZ Centrifuge Model 0406–2 operating at 4000 rpm for 15 min. This process resulted in deposition of the nanoparticles at the base of the centrifuge tubes with the nanofluid above it, the nanofluid was decanted and stored in a keg while the nanoparticles remained in the tubes. This process was repeated until the entire solution was centrifuged. The nanoparticles were calcined and upon further analysis with Digimizer™ image analysis software, particles with diameters ranging from 16 to 46 nm could be seen and an average particle diameter of 24.3886 nm was noted. The nanoparticles were then admixed with water as the base fluid at ten different concentrations as shown in Table 1. Corrosion tests was determined as described

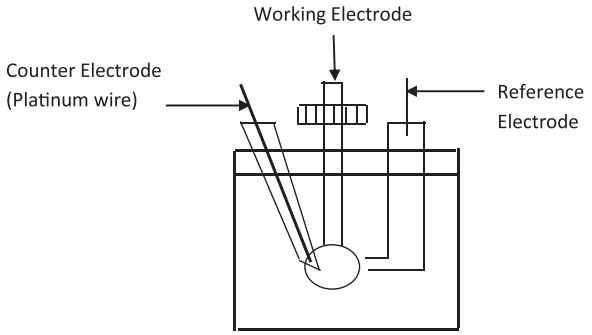

Fig. 1. Schematic of the electrochemical cell design for linear polarization tests.

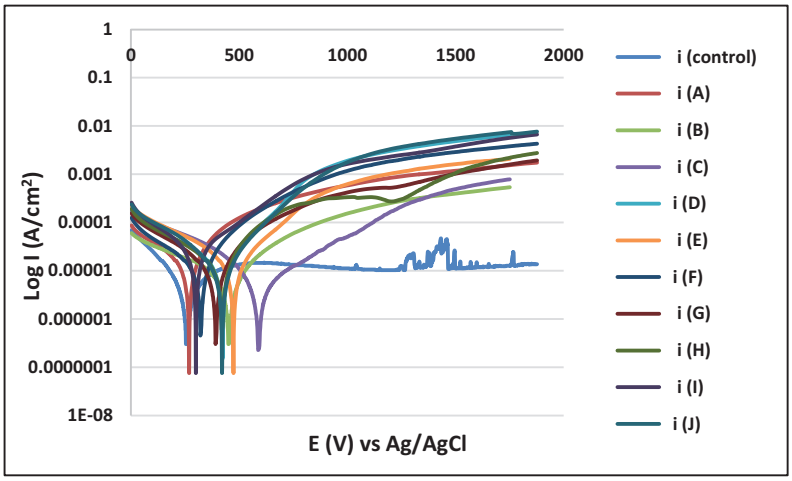

Fig. 2. Polarization behaviour of mild steel in RHA nano-coolant.

in [22]. The nano-fluid concentration was varied to mimic the various test environments. 11 mild steel plate samples of dimensions 20 mm x 20 mm were dry abraded with emery papers of 80, 180, 320 and 600 μm and thereafter immersed in 100 ml of the nano-fluid at different concentrations. Initial and final weights of mild steel coupons were recorded during the immersion test and the corrosion rate was calculated in mm/year via Eq. (1) [22,23].

$$\text{Corrosion Rate} = 87.6 \times \left(\frac{W}{DAT}\right) \tag{1}$$

Where D is metal density (g/cm^3), W is weight loss (mg), T is exposure time (hours), A is sample area (cm^2). Short lengths of copper wires were properly soldered to the samples used for the potentiodynamic polarization test before they were mounted in small cups of epoxy resins and left to cure for some time and then removed from the cups. The mounted samples were grinded to ensure the metal surface was properly exposed and then polished with emery paper up to 1200 grade. An electrochemical cell (Fig. 1) was setup comprising of the mounted sample (the working electrode), the silver-silver chloride (the reference electrode), the platinum electrode (the counter electrode) and the nano-coolant of varied concentration as the electrolyte. The electrochemical cell was connected to the DIGI-IVY Potentiostat to cause instantaneous corrosion using current and potential. The instantaneous corrosion rate was determined using linear polarization under aerated conditions of the electrochemical cell. The Open Circuit Potential (OCP) was first determined before conducting Linear Sweep Voltammetry (LSV). Duplicate experiments were carried out so as to determine the repeatability of the tests.

3. Data, value and validation

In this paper, the data described is from mass loss corrosion rate (Table 4), OCP (Table 5) and linear polarization (Fig. 2) of mild steel in RHA nano-coolant. The effect of the RHA nano-coolant was investigated by varying the concentration. For this data, linear polarization of mild steel samples was achieved by linear sweep voltammetry sandwiched between −0.875 V vs SCE to 1.0 V vs SCE. 0.15 mV/s was used for scanning. Table 1 shows the nano-fluid concentration for each test condition. Table 2 shows the compositional analysis of the nanoparticles from rice husk with silicon having the highest percentage composition of 45. This signifies that rice husk is rich in silicon Table 3.

Table 2
Compositional analysis of nano particles from rice husk.

ELEMENTS	COMPOSITION (%)
C	12.45
O	28.68
Na	3.09
Ca	2.28
Si	45.00
K	3.42
AL	2.15
Fe	1.43
Mg	1.90

Table 3
Compositional analysis of mild steel samples.

ELEMENTS	COMPOSITION (%)
C	0.11
Mn	0.47
Si	0.24
Cr	0.12
Ni	0.1
Mo	0.02
AL	0.03
Co	0.0012
Cu	0.14
W	0.06
V	0.003
Fe	Bal

Table 4
Immersion test results.

Sample(g/L)	24h	48h	Corrosion 72 h	Rate (mm/year) 96 h	120h	144 h	168h
RH-A	0.000302	0.000234	1.83E-05	2.06098E-05	9.89E-05	9.62E-05	2.75E-05
RH-B	0.000412	0.000151	9.16E-05	4.80896E-05	7.14E-05	0.000087	8.24E-05
RH-C	0.000137	8.24E-05	0.000101	0.000103049	0.000049	0.000060	0.000047
RH-D	0.00044	0.000151	0.000064	4.12196E-05	0.000077	0.000064	0.000043
RH-E	0.00033	0.000275	0.000073	3.43497E-05	0.000066	0.000055	0.000035
RH-F	0.000495	0.00011	0.000064	4.80896E-05	0.00011	0.000124	0.000018
RH-G	0.000357	0.000137	0.000082	0.000109919	0.000028	0.000037	0.000027
RH-H	0.00022	2.75E-05	0.000156	0.000144269	0.000049	0.000046	0.000047
RH-I	0.00011	0.000192	9.16E-05	7.55694E-05	0.000055	0.000055	0.000043
RH-J	0.001017	0.00066	0.000211	0.000144269	0.000198	0.000211	0.000298
RH-K	0.001017	0.00066	0.000211	0.000144269	0.000198	0.000211	0.000298

Table 4 shows the immersion test results gotten for mild steel with the RHA nano-coolant. The speed at which the mild steel material deteriorates in the nano-coolant is presented. This dataset determines the lifespan of mild steel in RHA nano-coolant. Maximum corrosion rate of 0.001017 mm/year was detected with the control test within 24 h. However, there is positive effect of RHA nanoparticle addition to the fluid. RH-F gave the lowest corrosion rate of 1.8E-05 mm/year at 168 h. This positive trend may be due to the unique favourable properties of RHA nanoparticles such as amazing surface effect, high functional density and large surface area. It was also observed that better protection of the material was achieved with increase in exposure time, hence lower corrosion rates.

Table 5 shows the OCP results. The OCP is the prospective of the mild steel specimen proportionate to the reference electrode at what time no current or potential is transmitted to the corrosion system. On the whole, the OCP of the working electrode is a thermodynamic factor which speaks about the thermodynamic propensity of mild steel to take part in the electrochemical corrosion reactions with the nano-coolant. Anodic and cathodic reactions are in equilibrium at OCP. There was alternating rise and fall in potential with increase in RHA concentration. Higher concentration of RHA (Sample H in particular) showed more positive potential values whereas lower concentration (Sample D) showed more noble behaviour. Fig. 2 shows the tafel plots of mild steel in RHA nano-coolant at 11 different concentrations including the control test situation. There was no distinct passivation exhibited by carbon steel in all the concentrations.

Declaration of Competing Interest

The authors declare that they have no known competing financial interests or personal relationships that could have appeared to influence the work reported in this paper.

Table 5
Open circuit potential results.

Time	V(V)	V(V)	V(V)	V(V)	V(V)	V(V)	V(V)	V(V)	V(V)	V(V)
(sec)	RH-A	RH-B	RH-C	RH-D	RH-E	RH-F	RH-G	RH-H	RH-I	RH-J
0.00	−0.54	−0.32	−0.37	−0.54	−0.39	−0.40	−0.41	−2.16	−0.54	−0.45
0.02	−0.54	−0.32	−0.37	−0.54	−0.39	−0.40	−0.41	−1.99	−0.54	−0.45
0.04	−0.54	−0.32	−0.37	−0.54	−0.39	−0.40	−0.41	−2.08	−0.54	−0.45
0.06	−0.54	−0.32	−0.37	−0.54	−0.39	−0.40	−0.41	−2.18	−0.54	−0.45
0.08	−0.54	−0.32	−0.37	−0.54	−0.39	−0.40	−0.41	−2.13	−0.54	−0.45
0.10	−0.54	−0.32	−0.37	−0.54	−0.39	−0.40	−0.41	−2.02	−0.54	−0.44
0.12	−0.54	−0.32	−0.37	−0.54	−0.39	−0.40	−0.41	−2.05	−0.54	−0.44
0.14	−0.54	−0.32	−0.37	−0.54	−0.39	−0.40	−0.41	−2.18	−0.54	−0.44
0.16	−0.54	−0.32	−0.37	−0.54	−0.39	−0.40	−0.41	−1.99	−0.54	−0.44
0.18	−0.54	−0.32	−0.37	−0.54	−0.39	−0.40	−0.41	−2.12	−0.54	−0.44
0.20	−0.54	−0.32	−0.37	−0.54	−0.39	−0.40	−0.41	−2.17	−0.54	−0.44
0.22	−0.54	−0.32	−0.37	−0.54	−0.39	−0.40	−0.41	−2.19	−0.54	−0.44
0.24	−0.54	−0.32	−0.37	−0.54	−0.39	−0.40	−0.41	−2.16	−0.54	−0.44
0.26	−0.54	−0.32	−0.37	−0.54	−0.39	−0.40	−0.41	−2.19	−0.54	−0.44
0.28	−0.54	−0.32	−0.37	−0.54	−0.39	−0.40	−0.41	−1.79	−0.54	−0.44
0.30	−0.54	−0.32	−0.37	−0.54	−0.38	−0.40	−0.41	−1.92	−0.54	−0.44
0.32	−0.54	−0.32	−0.37	−0.54	−0.38	−0.40	−0.41	−2.10	−0.54	−0.44
0.34	−0.54	−0.32	−0.37	−0.54	−0.38	−0.40	−0.41	−2.27	−0.54	−0.44
0.36	−0.54	−0.32	−0.37	−0.54	−0.38	−0.40	−0.41	−2.33	−0.54	−0.44
0.38	−0.54	−0.32	−0.37	−0.54	−0.38	−0.40	−0.41	−2.30	−0.54	−0.44
0.40	−0.54	−0.32	−0.37	−0.54	−0.38	−0.40	−0.41	−2.30	−0.54	−0.44
0.42	−0.54	−0.32	−0.37	−0.54	−0.38	−0.40	−0.41	−2.28	−0.54	−0.44
0.44	−0.54	−0.32	−0.37	−0.54	−0.38	−0.40	−0.41	−2.25	−0.54	−0.44
0.46	−0.54	−0.32	−0.37	−0.54	−0.38	−0.40	−0.41	−2.21	−0.54	−0.44
0.48	−0.54	−0.32	−0.37	−0.54	−0.38	−0.40	−0.41	−2.14	−0.54	−0.44
0.50	−0.54	−0.32	−0.37	−0.54	−0.38	−0.40	−0.41	−2.14	−0.54	−0.44
0.52	−0.54	−0.32	−0.36	−0.54	−0.38	−0.40	−0.41	−2.22	−0.54	−0.44
0.54	−0.54	−0.32	−0.36	−0.54	−0.38	−0.40	−0.41	−2.18	−0.54	−0.44
0.56	−0.54	−0.32	−0.36	−0.54	−0.38	−0.40	−0.41	−2.18	−0.54	−0.44
0.58	−0.54	−0.32	−0.36	−0.54	−0.38	−0.40	−0.41	−2.13	−0.54	−0.44
0.60	−0.54	−0.32	−0.36	−0.54	−0.38	−0.40	−0.41	−2.20	−0.54	−0.44
0.62	−0.54	−0.32	−0.36	−0.54	−0.38	−0.40	−0.41	−2.36	−0.54	−0.44
0.64	−0.54	−0.32	−0.36	−0.54	−0.38	−0.40	−0.41	−2.28	−0.54	−0.44
0.66	−0.54	−0.32	−0.36	−0.54	−0.38	−0.40	−0.41	−2.32	−0.54	−0.44
0.68	−0.54	−0.32	−0.36	−0.54	−0.38	−0.40	−0.41	−2.27	−0.54	−0.44
0.70	−0.54	−0.32	−0.36	−0.54	−0.38	−0.40	−0.41	−2.37	−0.54	−0.44
0.72	−0.54	−0.32	−0.36	−0.54	−0.38	−0.40	−0.41	−2.27	−0.54	−0.44
0.74	−0.54	−0.32	−0.36	−0.54	−0.38	−0.40	−0.41	−2.29	−0.54	−0.44
0.76	−0.54	−0.32	−0.36	−0.54	−0.38	−0.40	−0.41	−2.17	−0.54	−0.44
0.78	−0.54	−0.32	−0.36	−0.54	−0.38	−0.40	−0.41	−2.13	−0.54	−0.44
0.80	−0.54	−0.32	−0.36	−0.54	−0.38	−0.40	−0.41	−2.22	−0.54	−0.44
0.82	−0.54	−0.32	−0.36	−0.54	−0.38	−0.40	−0.41	−2.17	−0.54	−0.44
0.84	−0.54	−0.32	−0.36	−0.54	−0.38	−0.40	−0.41	−2.29	−0.54	−0.44
0.86	−0.54	−0.32	−0.36	−0.54	−0.38	−0.40	−0.41	−2.30	−0.54	−0.44
0.88	−0.54	−0.32	−0.36	−0.54	−0.38	−0.40	−0.41	−2.31	−0.54	−0.44
0.90	−0.54	−0.32	−0.36	−0.54	−0.38	−0.40	−0.41	−2.35	−0.53	−0.44
0.92	−0.54	−0.32	−0.36	−0.54	−0.38	−0.40	−0.41	−2.36	−0.53	−0.44
0.94	−0.54	−0.32	−0.36	−0.54	−0.38	−0.40	−0.41	−2.25	−0.53	−0.44
0.96	−0.54	−0.32	−0.36	−0.54	−0.38	−0.40	−0.41	−2.21	−0.53	−0.44
0.98	−0.54	−0.32	−0.36	−0.54	−0.38	−0.40	−0.41	−2.24	−0.53	−0.44
1.00	−0.54	−0.32	−0.36	−0.54	−0.38	−0.40	−0.41	−2.28	−0.53	−0.44
1.02	−0.54	−0.32	−0.36	−0.53	−0.38	−0.40	−0.41	−2.24	−0.53	−0.44
1.04	−0.54	−0.32	−0.36	−0.53	−0.38	−0.40	−0.41	−2.13	−0.53	−0.44
1.06	−0.54	−0.32	−0.36	−0.53	−0.38	−0.40	−0.41	−1.95	−0.53	−0.44
1.08	−0.54	−0.32	−0.36	−0.53	−0.38	−0.40	−0.41	−2.15	−0.53	−0.44
1.10	−0.54	−0.32	−0.36	−0.53	−0.38	−0.40	−0.41	−2.26	−0.53	−0.44
1.12	−0.54	−0.32	−0.36	−0.53	−0.38	−0.40	−0.41	−2.19	−0.53	−0.44
1.14	−0.54	−0.32	−0.36	−0.53	−0.38	−0.40	−0.41	−2.27	−0.53	−0.44
1.16	−0.54	−0.32	−0.36	−0.53	−0.38	−0.40	−0.41	−2.27	−0.53	−0.44
1.18	−0.54	−0.32	−0.36	−0.53	−0.38	−0.40	−0.41	−2.19	−0.53	−0.44
1.20	−0.54	−0.32	−0.36	−0.53	−0.38	−0.40	−0.41	−2.19	−0.53	−0.44
1.22	−0.54	−0.32	−0.36	−0.53	−0.38	−0.40	−0.41	−2.19	−0.53	−0.44
1.24	−0.54	−0.32	−0.36	−0.53	−0.38	−0.40	−0.41	−2.25	−0.53	−0.44
1.26	−0.54	−0.32	−0.36	−0.53	−0.38	−0.40	−0.41	−2.15	−0.53	−0.44
1.28	−0.54	−0.32	−0.36	−0.53	−0.38	−0.40	−0.41	−2.16	−0.53	−0.44
1.30	−0.54	−0.32	−0.36	−0.53	−0.38	−0.40	−0.41	−1.91	−0.53	−0.44
1.32	−0.54	−0.32	−0.36	−0.53	−0.38	−0.40	−0.41	−2.18	−0.53	−0.44
1.34	−0.54	−0.32	−0.36	−0.53	−0.38	−0.40	−0.41	−2.03	−0.53	−0.44

(*continued on next page*)

Table 5 (*continued*)

Time	V(V)	V(V)	V(V)	V(V)	V(V)	V(V)	V(V)	V(V)	V(V)	V(V)
1.36	−0.54	−0.32	−0.36	−0.53	−0.38	−0.40	−0.41	−2.07	−0.53	−0.44
1.38	−0.54	−0.32	−0.36	−0.53	−0.38	−0.40	−0.41	−2.17	−0.53	−0.44
1.40	−0.54	−0.32	−0.36	−0.53	−0.38	−0.40	−0.41	−2.09	−0.53	−0.44
1.42	−0.54	−0.32	−0.36	−0.53	−0.38	−0.40	−0.41	−2.07	−0.53	−0.44
1.44	−0.54	−0.32	−0.36	−0.53	−0.38	−0.40	−0.41	−2.07	−0.53	−0.44
1.46	−0.53	−0.32	−0.36	−0.53	−0.38	−0.40	−0.41	−2.09	−0.53	−0.44
1.48	−0.53	−0.32	−0.36	−0.53	−0.38	−0.40	−0.41	−2.16	−0.53	−0.44
1.50	−0.53	−0.32	−0.36	−0.53	−0.38	−0.40	−0.41	−2.20	−0.53	−0.44
1.52	−0.53	−0.32	−0.36	−0.53	−0.38	−0.40	−0.41	−2.10	−0.53	−0.44
1.54	−0.53	−0.32	−0.36	−0.53	−0.38	−0.40	−0.41	−2.11	−0.53	−0.44
1.56	−0.53	−0.32	−0.36	−0.53	−0.38	−0.40	−0.41	−2.11	−0.53	−0.44
1.58	−0.53	−0.32	−0.36	−0.53	−0.38	−0.40	−0.41	−2.05	−0.53	−0.44
1.60	−0.53	−0.32	−0.36	−0.53	−0.38	−0.40	−0.41	−2.22	−0.53	−0.44
1.62	−0.53	−0.32	−0.36	−0.53	−0.38	−0.40	−0.41	−2.21	−0.53	−0.44
1.64	−0.53	−0.32	−0.36	−0.53	−0.38	−0.40	−0.41	−2.11	−0.53	−0.43
1.66	−0.53	−0.32	−0.36	−0.53	−0.38	−0.40	−0.41	−2.06	−0.53	−0.43
1.68	−0.53	−0.32	−0.36	−0.53	−0.38	−0.40	−0.41	−2.11	−0.53	−0.43
1.70	−0.53	−0.32	−0.36	−0.53	−0.38	−0.40	−0.41	−2.18	−0.53	−0.43
1.72	−0.53	−0.32	−0.36	−0.53	−0.38	−0.40	−0.41	−2.08	−0.53	−0.43
1.74	−0.53	−0.32	−0.36	−0.53	−0.38	−0.40	−0.40	−2.16	−0.53	−0.43
1.76	−0.53	−0.32	−0.36	−0.53	−0.38	−0.40	−0.40	−2.18	−0.53	−0.43
1.78	−0.53	−0.32	−0.36	−0.53	−0.38	−0.40	−0.40	−2.05	−0.53	−0.43
1.80	−0.53	−0.32	−0.36	−0.53	−0.38	−0.40	−0.40	−2.13	−0.53	−0.43
1.82	−0.53	−0.32	−0.36	−0.53	−0.38	−0.40	−0.40	−2.12	−0.53	−0.43
1.84	−0.53	−0.32	−0.36	−0.53	−0.38	−0.40	−0.40	−2.04	−0.53	−0.43
1.86	−0.53	−0.32	−0.36	−0.53	−0.38	−0.40	−0.40	−2.03	−0.53	−0.43
1.88	−0.53	−0.32	−0.36	−0.53	−0.38	−0.40	−0.40	−2.11	−0.53	−0.43
1.90	−0.53	−0.32	−0.36	−0.53	−0.38	−0.40	−0.40	−2.15	−0.53	−0.43
1.92	−0.53	−0.32	−0.36	−0.53	−0.38	−0.40	−0.40	−2.12	−0.53	−0.43
1.94	−0.53	−0.32	−0.36	−0.53	−0.38	−0.40	−0.40	−2.03	−0.53	−0.43
1.96	−0.53	−0.32	−0.36	−0.53	−0.38	−0.40	−0.40	−2.02	−0.53	−0.43
1.98	−0.53	−0.32	−0.36	−0.53	−0.38	−0.40	−0.40	−2.01	−0.53	−0.43
2.00	−0.53	−0.32	−0.36	−0.53	−0.38	−0.40	−0.40	−1.99	−0.53	−0.43
2.02	−0.53	−0.32	−0.36	−0.53	−0.38	−0.40	−0.40	−2.03	−0.53	−0.43
2.04	−0.53	−0.32	−0.36	−0.53	−0.38	−0.40	−0.40	−2.01	−0.53	−0.43
2.06	−0.53	−0.32	−0.36	−0.53	−0.38	−0.40	−0.40	−2.05	−0.53	−0.43
2.08	−0.53	−0.32	−0.36	−0.53	−0.38	−0.40	−0.40	−1.99	−0.53	−0.43
2.10	−0.53	−0.32	−0.36	−0.53	−0.38	−0.40	−0.40	−2.06	−0.53	−0.43
2.12	−0.53	−0.32	−0.36	−0.53	−0.37	−0.40	−0.40	−2.15	−0.53	−0.43
2.14	−0.53	−0.32	−0.36	−0.53	−0.37	−0.40	−0.40	−2.14	−0.53	−0.43
2.16	−0.53	−0.32	−0.36	−0.53	−0.37	−0.40	−0.40	−2.10	−0.53	−0.43
2.18	−0.53	−0.32	−0.36	−0.53	−0.37	−0.40	−0.40	−2.13	−0.53	−0.43
2.20	−0.53	−0.32	−0.36	−0.53	−0.37	−0.40	−0.40	−2.11	−0.53	−0.43
2.22	−0.53	−0.32	−0.36	−0.53	−0.37	−0.40	−0.40	−2.17	−0.53	−0.43
2.24	−0.53	−0.32	−0.36	−0.53	−0.37	−0.40	−0.40	−2.19	−0.53	−0.43
2.26	−0.53	−0.32	−0.36	−0.53	−0.37	−0.40	−0.40	−2.31	−0.53	−0.43
2.28	−0.53	−0.32	−0.36	−0.53	−0.37	−0.40	−0.40	−1.75	−0.53	−0.43
2.30	−0.53	−0.32	−0.36	−0.53	−0.37	−0.40	−0.40	−1.60	−0.53	−0.43
2.32	−0.53	−0.32	−0.36	−0.53	−0.37	−0.40	−0.40	−1.84	−0.53	−0.43
2.34	−0.53	−0.32	−0.36	−0.53	−0.37	−0.40	−0.40	−1.94	−0.53	−0.43
2.36	−0.53	−0.32	−0.36	−0.53	−0.37	−0.40	−0.40	−1.84	−0.53	−0.43
2.38	−0.53	−0.32	−0.36	−0.53	−0.37	−0.40	−0.40	−1.90	−0.53	−0.43
2.40	−0.53	−0.32	−0.36	−0.53	−0.37	−0.40	−0.40	−2.00	−0.53	−0.43
2.42	−0.53	−0.32	−0.36	−0.53	−0.37	−0.40	−0.40	−1.91	−0.53	−0.43
2.44	−0.53	−0.32	−0.36	−0.53	−0.37	−0.40	−0.40	−1.75	−0.53	−0.43
2.46	−0.53	−0.32	−0.36	−0.53	−0.37	−0.40	−0.40	−1.67	−0.53	−0.43
2.48	−0.53	−0.32	−0.36	−0.53	−0.37	−0.40	−0.40	−1.75	−0.53	−0.43
2.50	−0.53	−0.32	−0.36	−0.53	−0.37	−0.40	−0.40	−2.08	−0.53	−0.43
2.52	−0.53	−0.32	−0.36	−0.53	−0.37	−0.40	−0.40	−1.93	−0.53	−0.43
2.54	−0.53	−0.32	−0.36	−0.53	−0.37	−0.40	−0.40	−2.04	−0.53	−0.43
2.56	−0.53	−0.32	−0.36	−0.53	−0.37	−0.40	−0.40	−1.71	−0.53	−0.43
2.58	−0.53	−0.32	−0.36	−0.53	−0.37	−0.40	−0.40	−1.80	−0.53	−0.43
2.60	−0.53	−0.32	−0.36	−0.53	−0.37	−0.40	−0.40	−1.92	−0.53	−0.43
2.62	−0.53	−0.32	−0.36	−0.53	−0.37	−0.40	−0.40	−1.61	−0.53	−0.43
2.64	−0.53	−0.32	−0.36	−0.53	−0.37	−0.40	−0.40	−1.95	−0.53	−0.43
2.66	−0.53	−0.32	−0.35	−0.53	−0.37	−0.40	−0.40	−1.92	−0.53	−0.43
2.68	−0.53	−0.32	−0.35	−0.53	−0.37	−0.40	−0.40	−1.94	−0.53	−0.43
2.70	−0.53	−0.32	−0.35	−0.53	−0.37	−0.40	−0.40	−2.22	−0.53	−0.43
2.72	−0.53	−0.32	−0.35	−0.53	−0.37	−0.40	−0.40	−2.00	−0.53	−0.43

(*continued on next page*)

Table 5 (*continued*)

Time	V(V)	V(V)	V(V)	V(V)	V(V)	V(V)	V(V)	V(V)	V(V)	V(V)
2.74	−0.53	−0.32	−0.35	−0.53	−0.37	−0.40	−0.40	−2.08	−0.53	−0.43
2.76	−0.53	−0.32	−0.35	−0.53	−0.37	−0.40	−0.40	−2.00	−0.53	−0.43
2.78	−0.53	−0.32	−0.35	−0.53	−0.37	−0.40	−0.40	−2.02	−0.53	−0.43
2.80	−0.53	−0.32	−0.35	−0.53	−0.37	−0.40	−0.40	−1.85	−0.53	−0.43
2.82	−0.53	−0.32	−0.35	−0.53	−0.37	−0.40	−0.40	−1.88	−0.53	−0.43
2.84	−0.53	−0.32	−0.35	−0.53	−0.37	−0.40	−0.40	−1.96	−0.53	−0.43
2.86	−0.53	−0.32	−0.35	−0.53	−0.37	−0.40	−0.40	−2.10	−0.53	−0.43
2.88	−0.53	−0.32	−0.35	−0.53	−0.37	−0.40	−0.40	−2.01	−0.53	−0.43
2.90	−0.53	−0.32	−0.35	−0.53	−0.37	−0.40	−0.40	−1.83	−0.53	−0.43
2.92	−0.53	−0.32	−0.35	−0.53	−0.37	−0.40	−0.40	−1.68	−0.53	−0.43
2.94	−0.53	−0.32	−0.35	−0.53	−0.37	−0.40	−0.40	−1.83	−0.53	−0.43
2.96	−0.53	−0.32	−0.35	−0.52	−0.37	−0.40	−0.40	−1.91	−0.53	−0.43
2.98	−0.53	−0.32	−0.35	−0.52	−0.37	−0.40	−0.40	−2.01	−0.53	−0.43
3.00	−0.53	−0.32	−0.35	−0.52	−0.37	−0.40	−0.40	−2.05	−0.53	−0.43

Acknowledgments

The authors are grateful to Covenant University for open access funding.

References

[1] K. Wickramasinghe, G. Perera, H. Herath, Formulation and performance evaluation of a novel coconut oil–based metalworking fluid, Mater. Manuf. Process. 32 (9) (2017) 1026–1033.
[2] J.D. Adámez, E. Samino, E. Sánchez, G.D. González, In vitro estimation of the antibacterial activity and antioxidant capacity of aqueous extracts from grape-seeds (Vitis vinifera L.), Food Control 24 (2012) 136–141.
[3] Y. Shokoohi, E. Khosrojerdi, B.R. Shiadhi, Machining and ecological effects of a new developed cutting fluid in combination with different cooling techniques on turning operation, J. Clean. Prod. 94 (2015) 330–339.
[4] S.A. Afolalu, O.D. Samuel, O.M. Ikumapayi, Development and characterization of nano-flux welding powder from calcined coconut shell ash admixture with FeO particles, J. Mater. Res. Technol. 9 (4) (2020) 9232–9241.
[5] S.A. Afolalu, G.E. Efekodha, S.O. Ongbali, A.A. Abioye, E.Y. Salawu, O.O. Ajayi, A.P. Oluwabunmi, Experimental analysis of the effect of tri-nano additives on wear rate of mild steel during machining, Proc. Manuf. 35 (2019) 395–400.
[6] Kalpakjian, S. 2013. Machining processes. In S. Kalpakjian, C. Fennel, R. Shivpuri, & O. Blodgett, Machining processes and machine tools (pp. 13–70).
[7] E. Brinksmeier, D. Meyer, A. Huesmann-Cordes, C. Herrmann, Metalworking fluids—mechanisms and performance, CIRP Ann. Manuf. Technol. 64 (2015) 605–628.
[8] J.E. Manikanta, B.N. Gupta, K.J.T. Manikanta, R Pradeep, Integrality characterization of machining with nano cutting fluids, Int. J. Mech. Eng. Technol. 10 (10) (2018) 1033–1042.
[9] J.S. Agapiou, Performance evaluation of cutting fluids with carbon nano-onions as lubricant additives, Proc. Manuf. 26 (2018) 1429–1440.
[10] S.A. Afolalu, S.O. Ongbali, A.A. Abioye, M.O. Udo, T.C. Akintayo, Experimental investigation of the effects of Bi-Nano additives on the mechanical properties of AISI 5130 mild steel during machining, Int. J. Mech. Eng. Technol. 9 (12) (2018) 264–274.
[11] S.A. Afolalu, A.A. Abioye, M.O. Udo, O.R. Adetunji, O.M. Ikumapayi, S.B. Adejuyigbe, Data showing the effects of temperature and time variances on Nano-additives treatment of mild steel during machining, Data Brief 19 (2018) (2018) 456–461.
[12] K.V. Wong, O. De Leon, Applications of nano-fluids: current and future, Adv. Mech. Eng. 2010 (2010) 1–11.
[13] M.A. Belewu, F.T. Babalola, Nutrient enrichment of some waste agricultural residues after solid state fermentation using Rhizopus oligosporus, J. Appl. Biosci. 13 (2009) 695–699.
[14] S. Maïga, S. Palm, C. Nguyen, G. Roy, N. Galanis, Heat transfer enhancement by using nanofluids in forced convection flow, Int. J. Heat Fluid Flow 26 (2005) 530–546.
[15] M.K. Gupta, M. Jamil, X. Wang, Q. Song, Z. Liu, M. Mia, … G.S. Imran, Performance evaluation of vegetable oil-based nano-cutting fluids in environmentally friendly machining of inconel-800 alloy, Materials 12 (2019) 2792.
[16] S.A. Afolalu, S.O. Ongbali, A.A. Abioye, M.O. Udo, T.C. Akintayo, Experimental investigation of the effects of Bi-Nano additives on the mechanical properties of AISI 5130 mild steel during machining, Int. J. Mech. Eng. Technol. 9 (12) (2018) 264–273.
[17] D. Thangadurai, J. Naik, M. David, J. Sangeetha, A.R.M.S. Al-Tawaha, Adetunji, … J.B. Adetunji, Nanomaterials from agrowastes: past, present and the future, Handbook of Nanomaterials and Nanocomposites for Energy and Environmental Applications, Springer Nature, Switzerland, 2020.
[18] I.C. Oladipo, S.B. Ogunsona, The utilization of agro-waste: a nanobiotechnology point of view, Recent Adv. Biol. Res. 5 (2019) 109–118.
[19] S.A. Afolalu, E.H. Asonaminasom, S.O. Ongbali, A.A. Abioye, M.O. Udo, E.Y. Salawu, Dataset on experimental investigation of optimum carburizing temperature and holding time of Bi-Nano additives treatment of AISI 5130 steel, Data Brief 19 (1) (2018) 2279–2283.
[20] M. Moradnazhad, O.U. Hakki, Energy efficiency of machining operations: a review, Proc. Inst. Mech. Eng. Part B J. Eng. Manuf. 231 (11) (2015) 1871–1889.
[21] ASTM G1-03, Standard practice for preparing, cleaning and evaluating corrosion test specimensAnnual Book of ASTM Standards, ASTM International, West Conshohocken, PA, USA, 2003.
[22] O.O. Joseph, C.A. Loto, S. Sivaprasad, J.A. Ajayi, S. Tarafder, Role of chloride in the corrosion and fracture behavior of micro-alloyed steel in E80 simulated fuel grade ethanol environment, Materials 9 (2016) 463.
[23] O.O. Joseph, C.A. Loto, S. Sivaprasad, J.A. Ajayi, O.S.I. Fayomi, Comparative assessment of the degradation mechanism of micro-alloyed steel in E20 and E80 simulated fuel ethanol environments, AIP Conf. Proc. 1758 (2016) 020019-1-9-6.